

Automatic measurement of surface runoff at the plot scale

Lucas Raimundo Rauber^{(1)*} , Dalvan José Reinert⁽¹⁾ , Paulo Ivonir Gubiani⁽¹⁾ ,
Kelvin Salbego Nunes⁽¹⁾  and Micael Stolben Mallman⁽¹⁾ 

⁽¹⁾ Universidade Federal de Santa Maria, Departamento de Solos, Santa Maria, Rio Grande do Sul, Brasil.

ABSTRACT: Although the hydrological importance of water infiltration into the soil and surface runoff is well known, manual measurement of these processes, especially at the plot and hillslope scales, is laborious and requires a trained team. This study aimed to develop prototypes with the *tipping bucket* principle for the automatic monitoring of surface runoff at a plot scale (14.5 × 3 m). In total, 18 prototypes were built and installed in an experiment with different soil covers. Aspects of the construction, calibration, operation and maintenance of the prototypes were reported in this study. Prototypes showed a satisfactory ability to monitor surface runoff with flow rates up to ~80 L min⁻¹. The devices have an adjustable resolution of up to 5 L pulse⁻¹, and they are inexpensive, easy to construct and simple to maintain. Although designed for a specific plot size (43.5 m²), the equipment can be adapted to smaller or larger plots by adjusting the volume of the tipping chambers. The proposed systems allow greater practicality in conducting experiments to monitor water loss through surface runoff at the plot scale and provide more detailed recordings of information.

Keywords: water infiltration, hydrograph, erosion, *tipping bucket*, datalogger.

* **Corresponding author:**

E-mail: rauber.lucas@acad.ufsm.br

Received: June 04, 2024

Approved: September 13, 2024

How to cite: Rauber LR, Reinert DJ, Gubiani PI; Nunes KS, Mallman MS. Automatic measurement of surface runoff at the plot scale. Rev Bras Cienc Solo. 2025;49:e0240102.

<https://doi.org/10.36783/18069657rbcs20240102>

Editors: José Miguel Reichert  and Jean Paolo Gomes Minella .

Copyright: This is an open-access article distributed under the terms of the Creative Commons Attribution License, which permits unrestricted use, distribution, and reproduction in any medium, provided that the original author and source are credited.



INTRODUCTION

Measurement of soil water infiltration and surface runoff is key in hydrological studies and for designing works to contain or control surface runoff (Assouline, 2013). The broad complexity of the surface hydrological processes that determine infiltration and surface runoff is better expressed in measurements performed at the scale of large plots (e.g., length between 11 and 22.1 m; width of 3 or 3.5 m) and/or hillslopes than in point-scale measurements (e.g., with infiltrometers or in small plots) (Langhans et al., 2019; Koppe et al., 2022).

In several countries, including Brazil (Anache et al., 2017), experience in measuring soil and water loss due to rainwater erosion at the plot scale was acquired from studies involving the application of the USLE (*Universal Soil Loss Equation*) and RUSLE (*revised version*) (Wischmeier and Smith, 1978; Renard et al., 1996). However, the measurements in these experiments are usually manual and laborious and require a trained team (Veiga and Wildner, 1993). In addition, only the accumulated soil and water losses (per event or annually) are quantified in these experiments. The relevant information that determines the hydrograph (e.g., time to ponding, initial abstraction depth, and maximum runoff rate), especially for natural rainfall events, is generally not recorded. Therefore, the automation of measurements would make these experiments more practical and contribute to a more detailed record of information.

Automatic measurements of surface runoff at the hillslope scale in southern Brazil have been performed with pressure transducers (Londero et al., 2021; Koppe et al., 2022). Using exams and flow rates discharged through gutters, the surface runoff variables can be obtained. However, the high acquisition cost of these transducers limits their use. In addition, the use of these sensors for surface runoff monitoring, especially in plot-scale experiments, has additional limitations. For example, the low volume of surface runoff in a plot compared with a hillslope (due to the difference in the area contributing to the surface runoff) can imply the low sensitivity of these systems in detecting oscillations in the surface runoff rate unless appropriate adaptations in gutter dimensions are performed.

An alternative and potential principle for automatically monitoring surface runoff at the plot scale is the *tipping bucket* (Edwards et al., 1974). This principle, for example, is widely used for the automatic measurement of hyetograms (Fankhauser, 1997) but has been much less explored for the automatic measurement of hydrographs. Despite the simple operation and low cost of acquisition or manufacture, the measurements by these systems have different types of associated errors (discussed in subsequent topics), which generates the need for adaptation and calibration of the prototypes to local conditions (e.g., hydrological characteristics and plot size) (Edwards et al., 1974; Wijayawardhana et al., 2021; Schwambach et al., 2023). Somavilla et al. (2019) proposed and calibrated a prototype with a *tipping bucket* system for automatically measuring surface runoff in small plots in southern Brazil (with a flow rate of $750 \times 10^3 \text{ mm}^3 \text{ min}^{-1}$). The proposition of prototypes with this principle to record the multiple variables of surface runoff at the scale of larger plots (in which experiments to measure soil and water loss by water erosion are usually conducted) has been much less explored, especially in Brazil. This study aimed to develop prototypes with a *tipping bucket* system for the automatic recording of surface runoff variables at the plot scale.

Tipping bucket: Operating principle

Equipment with a *tipping bucket* system for automatically recording water flow generally includes a pair of adjacent symmetrical chambers (Figure 1), which rotates around a central axis and to which rainwater or surface runoff is conducted (Edwards et al., 1974). When the rising water level in one of the chambers exceeds the position of the center of gravity of the chamber, the chamber tilts, and a new chamber is available to accumulate water (Edwards et al., 1974). The position of the center of gravity of the chambers depends

on factors such as (i) the dimensions of the chambers and (ii) the angle formed between the central axis of the tilting system and the stop (Figure 1).

The rainfall or runoff variables (e.g., total water depth and rate) are determined by quantifying the water storage capacity in each chamber (until tipping occurs) and the number of times the chambers tip over per time interval. The tilt count can be performed automatically with magnetic switches connected to microcontrollers or dataloggers (Figure 1). For example, the switch is usually fixed in front of or above the chambers and remains vertically aligned with the central axis of the tilting equipment (Figure 1). In addition, a magnet is attached to the chamber walls (Figure 1). The system records a pulse each time the chambers tilt, i.e., every time the magnet is attached to the chambers, it passes in front of the switch and generates continuity in the electrical current.

Associated errors and the need for calibration

The simplest way to calibrate equipment with the *tipping bucket* principle is to determine the volume of water required to cause each chamber to tilt. For example, water is added gradually (low and constant flow rates) to the equipment until each chamber tilts. Thus, a “static” or “quasistatic” resolution of the system (for example, L pulse⁻¹) is obtained (Edwards et al., 1974; Humphrey et al., 1997), which allows the determination of the rainfall variables or surface runoff, such as the flow rate (Equation 1).

$$Q_{sc} = \frac{\text{pulses}}{\Delta t} \times sc \quad \text{Eq. 1}$$

in which: Q_{sc} (L min⁻¹) is the estimated flow rate using the static resolution (sc) (L pulse⁻¹) and the number of pulses is the number of tilts accumulated in a given time interval (Δt) (min). Accumulated water depth (rain or surface runoff) is determined by integrating equation 1.

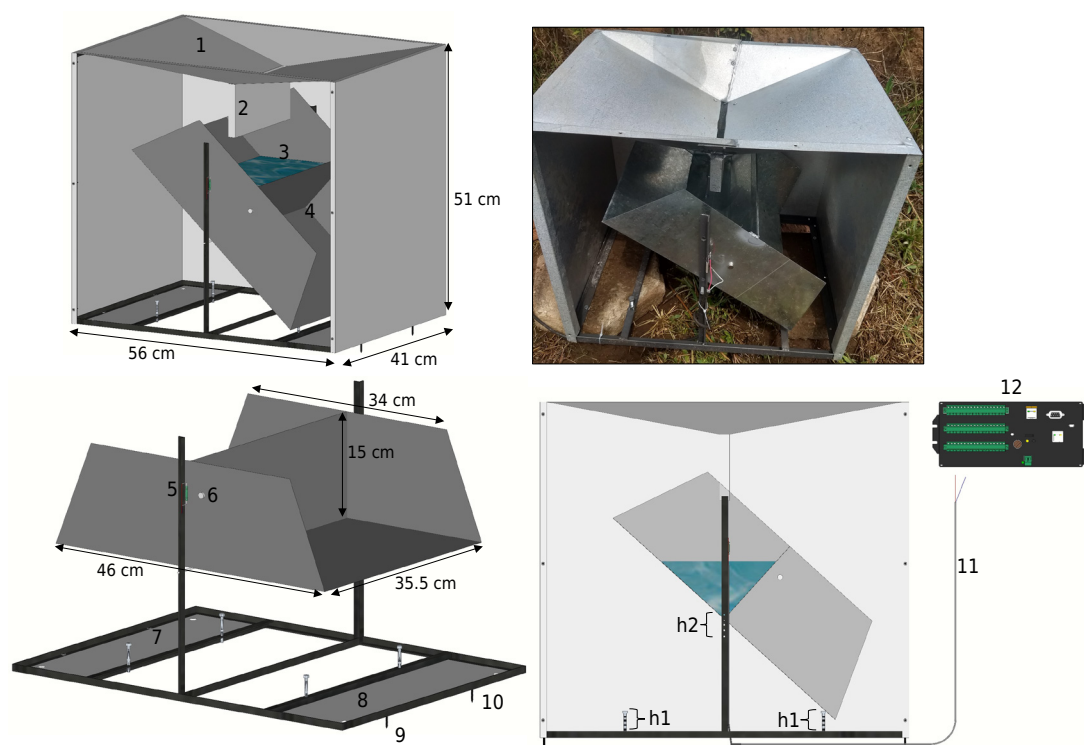


Figure 1. Components of the prototype with a *tipping bucket* system for automatic recording of surface runoff flow at plot scale with a maximum flow rate of $\sim 80 \text{ L min}^{-1}$. 1: water catchment and funneling area. 2: nozzle for discharging water into the internal chambers (3 and 4). 5: magnetic switch. 6: magnet. 7 and 8: plates for damping the impact of the water discharged by the chambers. 9 and 10: screws for securing the prototypes. 11: two-wire cable connecting the switch (5) to the datalogger (12). h1: screws for adjusting the height of the stopper (0 to 5 cm). h2: holes for adjusting the height of the tipping system axis (13 to 18 cm relative to the base of the prototype).

Despite the simple way of obtaining the rainfall or runoff variables with equation 1, the use of a static and fixed resolution, regardless of the applied flow rate, can generate inaccurate estimates of the rainfall or runoff variables (Edwards et al., 1974; Humphrey et al., 1997; Somavilla et al., 2019). For example, the water inlet nozzle in a system with chambers is usually aligned vertically with the axis of the tilting system (Figure 1). During the tipping of one chamber, water continues to accumulate until the wall of the other chamber exceeds the vertical axis of the nozzle, redirecting the flow exclusively to it. Thus, the higher the flow rate is, the greater the additional volume of water accumulated in the tilting chamber. Consequently, the total volume of water discharged by each chamber will be greater than that obtained by static calibration (at low flow rates), resulting in an underestimated flow (Edwards et al., 1974). Thus, for greater measurement accuracy, a calibration as a function of the applied flow is necessary, that is, one that establishes a dynamic resolution to the equipment.

Another concern in *tipping bucket* systems is related to the increase in the error of the flow estimate with increasing flow applied to the equipment (Edwards et al., 1974). For example, a more turbulent entry of water into the equipment with increased flow may cause premature or delayed tipping of the chambers. At the same time, the impact of the chambers with the stop can move the water level in the opposite chamber and influence the tipping, either anticipating or delaying it. This is particularly relevant in systems where the water capacity in each chamber exceeds 5 L (Edwards et al., 1974); dampening the impact of the chamber with the stopper is recommended in this case (Edwards et al., 1974). The higher the flow rate is, the greater the number of impacts of the chamber with the stopper per time interval, which potentially increases the measurement error. The quantification of the errors associated with these devices is thus essential to validate the prototypes and determine the flow rate range in which they provide precise and accurate measurements of surface runoff.

MATERIALS AND METHODS

Prototype proposition

Previous data of surface runoff flow from a plot area with dimensions of 14.5 × 3 m were considered for constructing the prototypes (description of the experiment in the subsequent topics). Chambers were designed to have a water storage capacity (up to tip) reaching ~ 5 L (0.11 mm depth considering the plot area, 43.5 m²) (Figure 1). The exact capacity of each chamber depends on the angle between the central axis of the tilting system and the stop, which can be adjusted in two ways: (i) by changing the height of the stop (adjustment of the vertical position of the screws) (Figure 1) or (ii) changing the vertical position of the tilting system axis (Figure 1). This possibility of adjusting the resolution of the system makes it possible to adapt each prototype slightly to the hydrological characteristics of each treatment (high or low susceptibility to surface runoff) and to the plot size. For example, for low surface runoff conditions (e.g., plots with high infiltration and high hydraulic resistance to surface runoff) or plots smaller than those considered in this study, increasing the resolution of the system (decreasing the volume of water that is discharged for each tilt) is suggested for a better characterization of the hydrograph.

In total, 18 prototypes with the same internal and external dimensions were built using angle iron and galvanized sheets (Figure 1). Lateral cladding of each prototype (with 4-mm thick galvanized sheets) was performed to minimize wind interference in the tilting system (Figure 1); for example, high wind speeds during storms could cause the chambers to tilt prematurely. On one of the front sides of each prototype (on the side where the switch and magnet were installed), a cover (4-mm thick galvanized sheet) was screwed to cover the box. This lining (cover) is easy to detach manually, allowing for resolution adjustment and maintenance of the internal system of the prototype (Figure 1). On the upper outer face of the prototypes, a 4-mm thick galvanized sheet

was used to create the funnel-flow structure and the nozzle (Figure 1). These structures conduct water to the internal tilting system, which is built with a 6-mm thick galvanized sheet (Figure 1). The nozzle covers almost the entire lateral dimension of the base of the chambers (Figure 1), which maximizes the uniformity in the distribution of water in the chambers and minimizes the turbulence of the water entry into the tilting system. At the bottom of each prototype, at the locations of projection of the water discharge from the chambers, galvanized plates (4-mm thick) were placed to cushion the impact of water with the concrete base (on which the prototypes are fixed) and the soil below (Figure 1). The direct impact of water on the soil could disrupt the soil and consequently displace the prototype from its original position, altering the resolution of the chambers.

The magnetic switch (Reed Switch 14 × 2 mm) was fixed to the front of the tipping chambers via plastic clamps (Figure 1). The magnet (Neodímio N50 Super Forte 10 mm × 4 mm) was attached to the sidewall of the tilting system, remaining approximately aligned with the center of the division of the chambers (Figure 1). A two-way shielded cable was used to connect the switch to the datalogger (CR1000) (Figure 1). The unit cost of each prototype, as of November 2021, was \$ 52.93 (considering a two-way cable length of 8 m). This includes (i) the material of the structure (angle iron and galvanized sheets) and specialized services for making the prototypes (\$ 48.33); (ii) a switch (\$ 1.15); (iii) a magnet (\$ 0.48); and (iv) a two-way cable (~ \$ 0.37 m⁻¹).

Calibration of prototypes in the field

Eighteen prototypes were frequently calibrated in the field (every 30 to 60 days), keeping them in the experimental position. The water that eventually accumulated in one of the chambers (from ineffective precipitation, for example) was initially discharged. Water was subsequently added with a graduated cylinder until each chamber tilted, and the volume used was recorded. Finally, the average static resolution of each prototype on each evaluation date was determined.

Calibration of prototypes in the laboratory

Dynamic calibration of the prototypes was performed in the Soil Physics and Hydraulics Laboratories of the Federal University of Santa Maria (UFSM). As all prototypes have the same dimensions, it was not necessary to establish an individual dynamic calibration for the 18 prototypes. The use of six prototypes was considered sufficient to establish a general dynamic calibration, which was applicable to the 18 prototypes.

Each prototype was initially set level on a bench to avoid shaking during testing. A PVC tube (diameter 100 mm) was coupled to a water pump to conduct water to the prototype; in the field, the flow is similar to that of the prototypes (Figure 2) (discussed in the next section). The equipment was subsequently subjected to different constant and known water flows (without sediment).

The first and lowest flow rates (~ 3 L min⁻¹; frequency ~ 0.8 pulses min⁻¹) were used for static calibration of each prototype. The time to accumulate four tilts (pulses) was recorded. The average volume of water corresponding to each tip was subsequently determined. This procedure was repeated three times. Consequently, the average static resolution of each prototype was obtained. To complement the data and perform a calibration as a function of the applied flow, another six flow rates (from 13 to ~ 80 L min⁻¹) were used. At each subsequent flow rate, the time for accumulating a certain number of pulses by the system (e.g., eight pulses for medium flows; 14 pulses for high flows) was recorded, and this process was repeated three times. Flow rates used corresponded to a frequency of up to 22 pulses min⁻¹ by the systems.

For each known flow rate added to each prototype (Q_{real}), equation 1 was used to estimate a corresponding flow rate (Q_{sc}). A polynomial equation between Q_{real} and Q_{sc} was subsequently fitted individually for each prototype and all the data (disregarding the

effect of the prototype). Thus, the final fit equations (Q_{dc}) (by prototype and general) were obtained. The prototypes were adjusted to initially exhibit a different static resolution (3 to 4 L pulse⁻¹) to analyze whether changes in the resolution of each system would imply the need for a specific dynamic calibration for each prototype.

Analysis of the functioning of the prototypes in the field

To analyze the operation of the equipment in the field, an experiment with six coverage conditions (species and intercrops of plants) and three replicates (18 plots in total) was used: T1 – exposed soil (with maintenance of surface crust); T2 – permanent grasses (*Paspalum notatum* predominant); T3 – intercropped black oat (*Avena strigosa*) and forage turnip (*Raphanus sativus*) in the winter followed by common bean (*P. vulgaris*) in the summer; T4 – Italian ryegrass (*Lolium multiflorum*) in the winter followed by common bean in the summer; T5 – intercropped black oat and vetch (*Vicia villosa*) in the winter followed by beans in the summer; and T6 – forage peanut (*Arachis pintoi*). The experiment is located in the Department of Soils of the UFSM (Federal University of Santa Maria; Rio Grande do Sul State) (Figure 2) and consists of continuous monitoring of surface runoff (from natural and simulated precipitation events) at the plot scale via the prototypes developed in this study (Figure 2). The soil in the area was classified as *Argissolo Vermelho-Amarelo Distrófico abruptico*, according to the Brazilian classification system (Santos et al., 2018), and as Psammentic Paleudult, according to the North American classification system (Soil Survey Staff, 2022). The effective vertical hydraulic conductivity of a saturated soil profile is 15 to 22 mm h⁻¹, indicating a relatively high susceptibility to surface runoff (Rauber, 2023). The plots measured 14.5 × 3 m (43.5 m²) and were delimited with metal plates; the largest dimension was oriented toward the slope, which was uniform and on the order of 6 % (± 0.70 %). Further information on the soil, treatments and history of the experimental area can be found in Rauber (2023).



Figure 2. Overview of the experiment at plot scale (14.5 × 3 m) with automatic surface runoff monitoring. 1: sprinklers used for precipitation simulation; 2: experimental plot with exposed soil; 3: PVC pipe for directing surface runoff to the prototype with a tipping bucket system (4), connected to a datalogger (5); 6: concrete base for securing the prototypes.

The generated flow in each plot was conducted by PVC pipes (100 mm in diameter) to the prototypes, which were fixed in level (screw to the concrete base) in front of the plots (Figure 2). The prototypes remained at a sufficiently low elevation in relation to the surface of the plots. This made it possible to conduct surface runoff via gravity to the automatic reading system (Figure 2). The devices were connected to CR1000 dataloggers programmed to record accumulated pulses every minute (Figure 1). A rain gauge connected to a CR1000 recorded the accumulated natural rainfall over the same interval.

Continuous monitoring of rainfall and runoff between 01/2022 and 01/2023 was performed. During this period, 37 effective natural precipitation events (with the generation of surface runoff in at least one plot of the treatment with exposed soil) were observed. In addition, 12 simulated precipitation events were performed (all effective in the generation of surface runoff). The simulator consists of a water pump and 180° SempreVerde/Fabrimar sprinklers arranged next to the plots (Figure 2). The area wetted by the irrigation system covered all the plots plus 3 m of border. The height of the falling water droplets was ~ 2.5 m. Simulated rainfall was monitored with collector cups (12 cups per plot) evenly distributed in each plot (covering water uptake in the upper, middle, and lower thirds of the plot). Total natural precipitation during the monitoring period was 1,420 mm, whereas the simulated precipitation was 1,790 mm.

An analysis of the equipment ability to record the hydrograph was performed considering representative and critical events of natural and simulated precipitation. For example, for each rainfall type (natural and simulated), the most critical event in generating surface runoff (with the highest accumulated surface runoff) was considered, as is the plot with the lowest resistance to surface runoff (one plot of the treatment with exposed soil). Thus, we analyzed the maximum error of the automatic measurements, as well as the adequacy of the resolution of the prototypes to the local hydrological conditions. The monitoring period also allows inference about aspects of equipment maintenance, such as the need to change switches and cabling and the need to clean the chambers.

Natural precipitation used to test the prototypes occurred on 09/01/2022. Accumulated rainfall was 35 mm, the duration was 3 h, and the maximum rainfall intensity for the 1-min period (minimum data acquisition interval) was 190 mm h⁻¹. The accumulated rainfall in the previous ten days (from natural and simulated events) was 205 mm (indicating high antecedent soil moisture). Simulated rainfall used to test the prototypes was performed on 01/10/2023. Rainfall intensity was constant at 63 mm h⁻¹ for 4 h, resulting in a cumulative amount of 252 mm. Accumulated rainfall in the previous ten days (from natural and simulated events) was 249 mm.

Prototypes installed in the field remain with the water catchment area (upper side of the equipment) directly exposed to rainfall (Figure 2). Therefore, the subtraction of the amount of additional water that enters the system by the rainfall in each data recording interval (1 min) is necessary. However, this amount of additional water is relatively small and does not imply extrapolation of the precision and accuracy of the equipment. Considering the water catchment area of each prototype (56 × 41 cm, 2,296 cm²), one pulse in the system is equivalent to a rainfall depth of ~ 17 mm. An expressively high precipitation peak, 190 mm h⁻¹, for example, generates an increase in flow of only 0.73 L min⁻¹. On the other hand, if the surface runoff flow rate is 1, 5, 20 or 50 L min⁻¹, this rainfall intensity (190 mm h⁻¹) adds 73, 15, 3.6, and 1.5 % to the flow, respectively.

Statistical analysis

Willmott index of agreement was used to analyze the correspondence between actual flow and estimated flow (by static and dynamic resolution). Percent Bias (P_{bias}) was used to analyze the trends of overestimation or underestimation of the real flow, whereas the root mean square error (RMSE) was used to analyze the average deviation between the actual and estimated values of flow. Residuals of the dynamic calibration equations

were analyzed graphically via the Shapiro–Wilk (distribution normality), Durbin–Watson (independence) and Breusch–Pagan (variance homogeneity) tests. All statistical procedures were performed in the R environment (R Development Core Team, 2022).

RESULTS AND DISCUSSION

Calibration

Results confirmed the need to use a dynamic calibration (as a function of flow rate) of the prototypes (Figure 3). Table 1 presents the coefficients and statistics of the dynamic calibration adjustments (general and individual for each prototype). When the flow rate was estimated using only the static resolution of each prototype, that is, disregarding the effect of the flow rate on the resolution of the prototypes (Equation 1), the actual flow rate was underestimated by an average of 8 % (Table 2). In addition, the deviation between the actual flow and the flow estimated by the static resolution increased with increasing applied flow (Figure 3); for example, it reached ~ 25 % at the highest flow rate used (~ 80 L min⁻¹) (Figure 3). Willmott index values of ~ 0.9 reflect the low agreement between the actual and estimated flow rates according to equation 1 (static resolution) (Table 2). General polynomial equation between the real flow and Q_{sc} , on the other hand, fits the data well and can be used for dynamic and final calibrations of the prototypes (Q_{dc}) (Figure 3; Table 1). When the entire range of Q_{real} values (up to ~ 80 L min⁻¹) is considered, the RMSE (1.77 L min⁻¹) of the general Q_{dc} is relatively low, at ~ 2 % (Table 1). In addition, the Q_{dc} values strongly agreed with the real flow values (Willmott of ~ 0.98), with no tendency to overestimate or underestimate (mean P_{bias} of -0.01) (Table 2). The model residual, however, decreases considerably (~ 55 %) when a specific dynamic calibration equation is used for each prototype, possibly because of the specific static resolution of each system (Table 1).

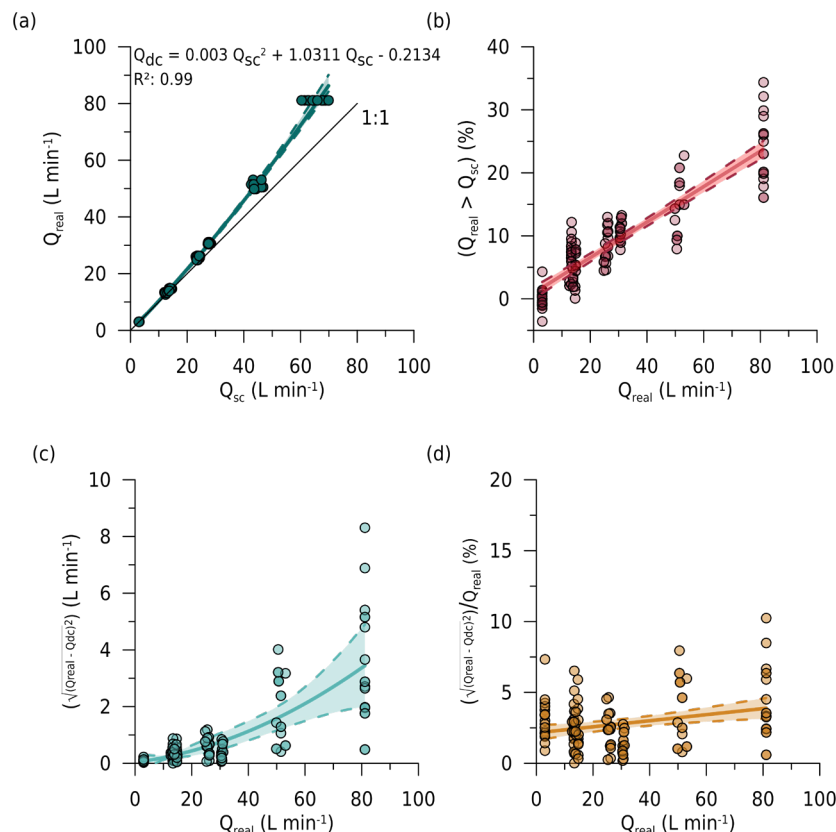


Figure 3. Relationship between the flow rate applied to the equipment (Q_{sc}) and the flow rate estimated by the equipment using static resolution (Q_{dc}), with the respective adjustment equation (dynamic calibration - Q_{dc}) (a). Percentage by which Q_{real} exceeds Q_{dc} as a function of the magnitude of Q_{real} (b). Absolute (c) and relative (d) residuals between Q_{real} and Q_{dc} (as shown in graph “a”) as a function of the magnitude of Q_{real} . Analysis considering the six prototypes. n: 126.

Table 1. Coefficients and adjustment statistics of the dynamic calibration for each prototype to estimate surface runoff flow rate (L min^{-1})

Prototype	Coefficients			n	p-value	R ²	RMSE	Norm	Ind	Hom
	Intersection	Q _{sc}	Q _{sc} ²						p-value	
L min ⁻¹										
1	0.316	0.930	0.006	21	<2.2E-16	0.99	0.69	0.036	0.550	0.005
2	0.843	0.958	0.003	21	<2.2E-16	0.99	1.13	0.076	0.334	0.052
3	0.541	0.943	0.003	21	<2.2E-16	0.99	0.77	0.655	0.182	0.014
4	0.113	0.999	0.004	21	<2.2E-16	0.99	0.59	0.005	0.852	0.095
5	0.389	0.953	0.004	21	<2.2E-16	0.99	0.60	0.103	0.046	0.039
6	-1.073	1.131	0.001	21	<2.2E-16	0.99	1.02	0.001	0.104	0.370
General*	-0.213	1.031	0.003	126	<2.2E-16	0.99	1.77	<0.001	0.730	<0.001

Q_{sc} : flow rate estimated by equation 1 (L min^{-1}), i.e., using the static resolution of each prototype. RMSE: root mean square error. Norm: normality of the residuals. Ind: independence of the residuals. Hom: homoscedasticity of the residuals. *: equation considering data from all prototypes.

Table 2. Static resolution of each prototype and Willmott's concordance index and Percent Bias (P_{bias}) between actual flow rate and estimated flow rate

Prototype	Resolution	Q_{sc}		Q_{dc}	
		Willmott	P_{bias}	Willmott	P_{bias}
L pulse ⁻¹					
1	4.03	0.876	0.097	0.988	-0.006
2	3.53	0.903	0.089	0.979	-0.027
3	3.90	0.920	0.064	0.984	-0.015
4	3.28	0.882	0.099	0.990	-0.006
5	3.00	0.901	0.080	0.989	-0.010
6	3.03	0.910	0.076	0.983	0.023
General*	3.46	0.899	0.084	0.974	0.003

Q_{sc} : flow rate estimated by equation 1, i.e., using the static resolution of each prototype (Table 1). Q_{dc} : flow rate estimated by dynamic calibration (Table 1). *: equation considering data from all prototypes.

As expected, the variance of the Q_{dc} residue increased with increasing applied flow (Figure 3c). In addition, although independent, the residues of this equation did not have a normal distribution (Table 1). The mean deviation from the estimate was 0.35 L min^{-1} for flow rates up to $\sim 30 \text{ L min}^{-1}$ but increased to 3.5 L min^{-1} at flow rates of $\sim 80 \text{ L min}^{-1}$ (Figure 3c). On the other hand, using a specific dynamic calibration for each prototype slightly attenuated this problem (Table 1). For example, of the six specific dynamic calibrations, three presented homogeneous variance ($p > 0.05$) (Table 1). However, the trend of the relative error of the general dynamic calibration remained between 2 and 3 % throughout the domain range of the flow values (Figure 3d). This demonstrates the adequate capacity of the equipment to monitor flow rates up to $\sim 80 \text{ L min}^{-1}$. Flow rates above this limit, however, might compromise the precision and accuracy of the equipment. General dynamic calibration (equation in figure 3a), obtained via six prototypes, allows satisfactory estimates of surface runoff for the 18 prototypes developed in this study. However, each prototype requires a specific static calibration.

Operation and maintenance of prototypes in the field

Prototypes showed satisfactory ability to monitor surface runoff in the field under natural and simulated rainfall (Figure 4). The resolution of the equipment and the discretization of the time for recording the data (1 min) satisfactorily detected the fluctuations in the surface runoff flow (Figure 4). Peaks of high-intensity precipitation ($> 100 \text{ mm h}^{-1}$) are usually of short duration (6 to 7 min for the Santa Maria region) (Mehl et al., 2001), which

reinforces the need for high-time discretization for data recording (Figure 4). On the other hand, a high frequency of data recording can generate high irregularity in the estimated flow (Figure 4). For example, as the pulse count time interval is fixed and predefined (1 min, for example), the water accumulated in one of the chambers at the end of the first time interval may be counted only in the following time interval. This may result in a higher pulse count in the second interval, even when the flow rate is constant. The eventual disparity in the resolution of each of the chambers may have contributed to this irregularity in the estimated flow. Although negligible, this flow irregularity can be mitigated by using the moving average of the flow values (every five values, for example).

Precipitation events show an important contrast in the “operating mode” of precipitation in the surface runoff (Figure 4). In natural precipitation, for example, surface runoff seems to be predominantly due to the high magnitude of the maximum intensity of precipitation (Figure 4). In the simulated event, on the other hand, the runoff depends more on the accumulated precipitation (Figure 4). Therefore, it seems that the prototypes were adequately sized at the plot scale (43.5 m^2) and were adapted to a wide variety of rainfall characteristics. The observed runoff flows (maximum runoff rates between 40 and 50 L min^{-1} for the natural event and $\sim 30 \text{ L min}^{-1}$ for the simulated event) (Figure 4) are within the calibration domain and within a range in which the errors are relatively and absolutely low (Figure 3). In addition, the equipment was simple and inexpensive to maintain. Eventually, replacing the magnetic switches, which have low acquisition and installation costs was necessary.

The analysis of the functioning of the prototypes under natural and simulated rainfall reinforces the need to use dynamic calibration to avoid underestimating the surface runoff variables (Figure 4; Table 3). For example, in a natural event, the main variable underestimated when only the static resolution of the system was used in the calculation

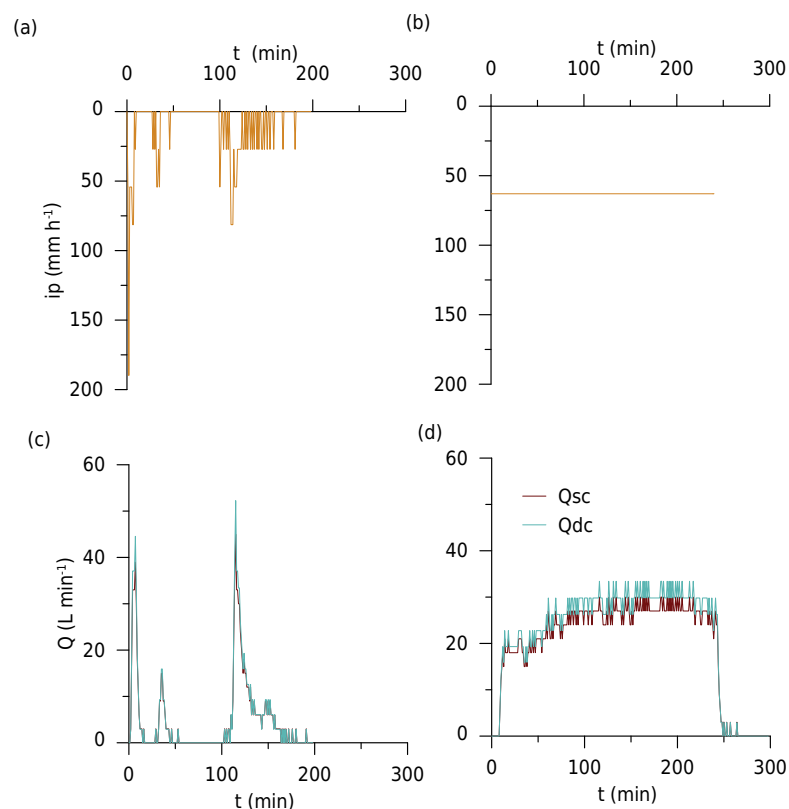


Figure 4. Hyetograph of natural precipitation (a) and simulated precipitation (b). Corresponding hydrograph for natural precipitation (c) and simulated precipitation (d). Q_{sc} : surface runoff flow rate estimated using equation 1, that is, utilizing the static resolution of the prototype; Q_{dc} : surface runoff flow rate estimated using the dynamic calibration equation (equation from Figure 3a); ip : precipitation intensity; Q : surface runoff flow rate; t : time.

(Equation 1) was the maximum runoff rate (Table 3). In the simulated event, on the other hand, surface runoff depth was the main underestimated variable (Table 3). In addition, although designed for a specific plot size (14.5×3 m), the prototypes would probably work properly in larger plots (e.g., 22.1×3 m) or smaller plots (e.g., 11×3 m), provided that the flow remained under the dynamic calibration domain range. For larger plots, it would still be possible to use flow dividers or increase the volume of the chambers to better adapt the flow to the calibration domain range (Wijayawardhana et al., 2021).

The construction of an impact damping system between the chambers and the stops was unnecessary. The very evident sound emitted by the impact of the chambers with the stops, without the damping system, allowed monitoring of the operation of the tilting system in the field during storms, even with the prototypes fully coated laterally and without visual contact with the chambers (Figure 2).

Other errors associated with the measurements

The impact of the chambers with stops (Figure 1) and/or sediment accumulation in the chambers can change the static resolution of prototypes installed in the field (Wijayawardhana et al., 2021). This generates the need to recalibrate equipment in the field, especially in times of more intense and frequent rainfall (Wijayawardhana et al., 2021). However, the change in the static resolution of the prototypes overtime was only 3.6 % in this study (average of five well-distributed evaluation periods over one year; 18 prototypes). The increase in the capacity of one of the chambers (volume of water until tipping occurs) can eventually be offset by the decrease in the capacity of the other. Consequently, the average static resolution of the chambers slightly changes. The tilting system is adjusted so that each chamber has a similar capacity for discharging water. A small disparity, however, is probably negligible.

Water accumulating in one of the chambers before the event starts (from the previous event or due to ineffective precipitation accumulated in the chamber, for example) can cause overestimation of the accumulated surface runoff. On the other hand, if the amount of water that enters the tipping system at the end of the precipitation event is lower than the resolution of the system, the quantification of this amount will not be performed, resulting in underestimation of the accumulated surface runoff. However, the proportion of this error decreases significantly as the accumulated surface runoff and plot size increase (Somavilla et al., 2019). Considering a resolution of 4 L pulse⁻¹ and a plot size of 43.5 m², for example, this error could reach 9, 1.8, 0.5 and 0.2 % for accumulated surface runoffs of 1, 5, 20 and 50 mm, respectively.

Calibration of the prototypes was performed without the presence of sediment in the water. Therefore, if the density of suspended material is greater than that of water, an increase in its concentration increases the mass per unit volume of runoff. Consequently, this may cause the chambers to tilt prematurely. However, the sediment concentration usually present in runoff is likely negligible enough to affect the static or dynamic resolution of the equipment. On the other hand, this could be investigated in subsequent studies.

Table 3. Precipitation and estimated surface runoff for natural and simulated precipitation events

Type of P	P	ip_{max}	Q_{max}			R		
			sc	dc	dc > sc	sc	dc	dc > sc
	mm		mm h ⁻¹		%	mm		%
Natural	35	190	62	72	16	23	24	4
Simulated	252	63	37	41	11	135	148	10

P: accumulated precipitation; ip_{max} : maximum precipitation intensity for a 1-minute period (minimum data recording interval); Q_{max} : maximum surface runoff rate for a 1-minute period; R: accumulated surface runoff; sc: estimate using equation 1, i.e., utilizing the static resolution of the prototype; dc: estimate using the dynamic calibration of the prototype (equation from Figure 3a).

CONCLUSIONS

Prototypes with the *tipping bucket* principle for the automatic recording of surface runoff at the plot scale were developed and calibrated in this study. The systems are simple to operate, practical, inexpensive, and easy to build and maintain. The prototypes can automatically monitor runoff flows up to $\sim 80 \text{ L min}^{-1}$. However, disregarding the runoff rate effect on the systems resolution leads to an underestimation of the surface runoff. Although designed for a specific plot size ($14.5 \times 3 \text{ m}$), the systems adapt well to slightly smaller or slightly larger plots. These systems are expected to enable more practicality in conducting experiments to monitor water loss by surface runoff at the plot scale and provide more detailed records of information.

DATA AVAILABILITY

The data will be provided upon request.


FUNDING



We would like to thank the Coordenação de Aperfeiçoamento de Pessoal de Nível Superior (CAPES) for the scholarship granted to the first author – Finance Code 001.





ACKNOWLEDGMENTS

We would like to thank Mr. Aládio Moraes de Lima for his great effort and dedication in constructing the prototypes developed in this study.

AUTHOR CONTRIBUTIONS




Conceptualization:  Dalvan José Reinert (equal) and  Lucas Raimundo Rauber (equal).

Investigation:  Kelvin Salbego Nunes (equal) and  Lucas Raimundo Rauber (equal).




Methodology:  Dalvan José Reinert (equal),  Kelvin Salbego Nunes (equal),  Lucas Raimundo Rauber (equal) and  Micael Stolben Mallman (equal).

Supervision:  Dalvan José Reinert (equal).

Validation:  Lucas Raimundo Rauber (equal).

Visualization:  Dalvan José Reinert (equal),  Lucas Raimundo Rauber (equal) and  Paulo Ivonir Gubiani (equal).

Writing - original draft:  Lucas Raimundo Rauber (equal).

Writing - review & editing:  Dalvan José Reinert (equal),  Micael Stolben Mallman (equal) and  Paulo Ivonir Gubiani (equal).

REFERENCES

- Anache JAA, Wendland EC, Oliveira PTS, Flanagan DC, Nearing MA. Runoff and soil erosion plot-scale studies under natural rainfall: A meta-analysis of the Brazilian experience. *Catena*. 2017;152:29-39. <https://doi.org/10.1016/j.catena.2017.01.003>
- Assouline S. Infiltration into soils: Conceptual approaches and solutions. *Water Resour Res*. 2013;49:1755-72. <https://doi.org/10.1002/wrcr.20155>

- Edwards IJ, Jackson WD, Fleming PM. Tipping bucket gauges for measuring run-off from experimental plots. *Agr Meteorol.* 1974;13:189-201.
[https://doi.org/10.1016/0002-1571\(74\)90046-6](https://doi.org/10.1016/0002-1571(74)90046-6)
- Fankhauser R. Measurement properties of tipping bucket rain gauges and their influence on urban runoff simulation. *Water Sci Technol.* 1997;36:7-12.
[https://doi.org/10.1016/S0273-1223\(97\)00625-2](https://doi.org/10.1016/S0273-1223(97)00625-2)
- Humphrey MD, Istok JD, Lee JY, Hevesi JA, Flint AL. A new method for automated dynamic calibration of tipping-bucket rain gauges. *J Atmos Ocean Tech.* 1997;14:1513-9.
[https://doi.org/10.1175/1520-0426\(1997\)014<1513:ANMFAD>2.0.CO;2](https://doi.org/10.1175/1520-0426(1997)014<1513:ANMFAD>2.0.CO;2)
- Koppe E, Schneider FJA, Londero AL, Queiroz R, Buligon L, Minella JPG. Soil water infiltration evaluation from punctual to hillslope scales. *Environ Monit Assess.* 2022;194:300.
<https://doi.org/10.1007/s10661-022-09893-x>
- Langhans C, Diels J, Clymans W, van den Putte A, Govers G. Scale effects of runoff generation under reduced and conventional tillage. *Catena.* 2019;176:1-13.
<https://doi.org/10.1016/j.catena.2018.12.031>
- Londero AL, Minella JPG, Schneider FJA, Deuschle D, Menezes D, Evrard O, Boeni M, Merten GH. Quantifying the impact of no-till on runoff in southern Brazil at hillslope and catchment scales. *Hydrol Process.* 2021;35:e14286. <https://doi.org/10.1002/hyp.14094>
- Mehl HU, Eltz FLF, Reichert JM, Didoné IA. Caracterização de padrões de chuvas ocorrentes em Santa Maria (RS). *Rev Bras Cienc Solo.* 2001;25:475-83.
<https://doi.org/10.1590/S0100-06832001000200023>
- R Development Core Team. R: A language and environment for statistical computing. Vienna, Austria: R Foundation for Statistical Computing; 2022. Available from: <http://www.R-project.org/>.
- Rauber LR. Plantas de cobertura e umidade antecedente afetam a infiltração de água em um Argissolo [thesis]. Santa Maria, RS: Universidade Federal de Santa Maria; 2023.
- Renard KG, Foster GR, Weesies GA, McCool DK, Yoder DC. Predicting soil erosion by water: A guide to conservation planning with the Revised Universal Soil Loss Equation (RUSLE). Washington, DC: United States Department of Agriculture. 1996. (Agriculture Handbook, 703).
- Santos HG, Jacomine PKT, Anjos LHC, Oliveira VA, Lumbreiras JF, Coelho MR, Almeida JA, Araújo Filho JC, Oliveira JB, Cunha TJF. Sistema brasileiro de classificação de solos. 5. ed. rev. ampl. Brasília, DF: Embrapa; 2018.
- Schwamback D, Persson M, Berndtsson R, Anache JAA, Wendland EC. Adaptive design of tipping bucket flow meters for continuous runoff measurement. *Front Environ Sci.* 2023;11:1286929.
<https://doi.org/10.3389/fenvs.2023.1286929>
- Soil Survey Staff. Keys to soil taxonomy. 13th ed. Washington, DC: United States Department of Agriculture, Natural Resources Conservation Service; 2022.
- Somavilla A, Gubiani PI, Zwirtz AL. Tipping bucket prototype for automatic quantification of surface runoff rate in plots. *Rev Bras Cienc Solo.* 2019;43:e0180096.
<https://doi.org/10.1590/18069657rbcs20180096>
- Veiga M, Wildner LP. Manual para la instalacion y conduccion de experimentos de perdida de suelos. Santiago, Chile: Proyecto Regional FAO; 1993.
- Wijayawardhana LMJR, Weerasinghe KDN, Navaratne CM. Tipping bucket device for measuring runoff in small catchments. *Hydrol Sci J.* 2021;66:2258-66.
<https://doi.org/10.1080/02626667.2021.1977307>
- Wischmeier WH, Smith DD. Predicting rainfall erosion losses - a guide to conservation planning. Washington, DC: United States Department of Agriculture, Natural Resources Conservation Service; 1978.